Local response of W-shaped steel columns under blast loading

Kyungkoo Lee

Department of Architectural Engineering, Seoul National University, Seoul 151-742, Korea

Taejin Kim and Jinkoo Kim[†]

Department of Architectural Engineering, Sungkyunkwan University, Suwon 440-746, Korea

Abstract. Local failure of a primary structural component induced by direct air-blast loading may be itself a critical damage and lead to the partial or full collapse of the building. As an extensive research to mitigate blast-induced hazards in steel frame structure, a state-of-art analytical approach or high-fidelity computational nonlinear continuum modeling using computational fluid dynamics was described in this paper. The capability of the approach to produce reasonable blast pressures on a steel wide-flange section column was first evaluated. Parametric studies were conducted to observe the effects of section sizes and boundary conditions on behavior and failure of columns in steel frame structures. This study shows that the analytical approach is reasonable and effective to understand the nature of blast wave and complex interaction between blast loading and steel column behavior.

Keywords: computational fluid-dynamics; fluid-structure interaction; blast load; steel column.

1. Introduction

Blast explosions induced by accidents or intentional attacks have resulted in severe damage to buildings and extreme casualties all over the world. There has been relatively a little study on the safety of the damaged building after an explosive event because it is a priority to prevent the event with precaution. However, a terrorist attack against the World Trade Center buidlings in New York City on September 11, 2001 aroused huge interest from structural engineers and researchers in blast-related research and blast resistant design approach for private buildings, especially high rise buildings.

The most effective way to minimize the injuries due to blast loading is to secure sufficient stand-off distance between an explosive and a target structure and reduce the magnitude of the blast shock wave so that the structure are not highly damaged. However, there is a need for evaluating various expected blast loading scenarios (based on explosive size, distance from the detonation, building shape, etc.) because adequate standoff to limit the approach may not be acquired due to building

---

† Associate Professor, Corresponding author, E-mail: jkim12@skku.edu

location or other constructional circumstances. Even though the severity and amount of damage in buildings and casualties due to an explosive event cannot be predicted with certainty, general indication of the overall level of damages can be given in an explosive event.

Building damage caused by an explosive blast may be divided into local failure (direct blast effects) and progressive building collapse (consequential effects). Direct blast effects are that the highly intensive blast pressures induce localized failure of structural components such as exterior walls, windows, columns, beams, and floor systems. Consequential effects are that the local failure of primary structural members, especially columns resisting the building gravity loads, redistributes excessive gravity loads to adjacent members because of loss of their resistance, which leads to partial or total progressive building collapse.

Currently blast-resistant design is generally carried out by simplifying the models and conducting static analysis, single degree-of-freedom dynamic analysis, or rigid-plastic analysis (Kang and Liew 2006). However, because of the diversity of blast loading scenarios and the complexity of response mechanisms of components and their assemblages, the development of the design practice involving sophisticated numerical methods as well as empirical and analytical methods has been required in this field (Marchand and Alfawakhiri 2005).

Meanwhile, wind or earthquake-resistant steel frames may resist a credible blast loading without lateral instability or collapse (Hamburger and Whittaker 2003). Nevertheless, a huge or close-to-structure explosion will cause extreme damage of main structural components and the entire loss of gravity load-carrying capacity of vertical components. Blast resistant design of steel frames generally provides sufficient toughness of components and structural system capable of limiting the possibility of building collapse (Hamburger and Whittaker 2003). Therefore, simulation of blast loading and estimation of column behaviour and damage under blast loading are very important phase of research to evaluate the resistance and safety of building against direct and consequential blast damage.

The goal of this paper is to observe the behavior of wide flange section column subjected to blast load as a part of extensive research to mitigate blast-induced hazards in steel frame structure. High-fidelity computational nonlinear dynamic continuum analysis using computational fluid dynamics (CFD) was performed and its capability to estimate blast pressures on a structure was evaluated. Then, the effects of section sizes and boundary conditions on behavior and failure of steel columns were studied.

2. Blast loads acting on a structure

2.1 Characteristics of blast load

Explosion dissipates energy forming light, sound, and very dense and high pressure wave with intial expansion at very high velocities. Typical explosive detonations in the free field create a suddenly rising and rapidly decaying pressure to satisfy equilibrium with surrounding air, or a shock wave with very short duration. The range in which the risen pressure decays back to ambient pressure is defined as a positive phase (see Fig. 1). As the wave front expands, a negative pressure phase occurs when the pressure is lower than ambient pressure. The negative phase has a little effect on the response of structures (FEMA-426, 2003).

Blast wave is reflected and amplified when the incident pressure wave is transferred through air
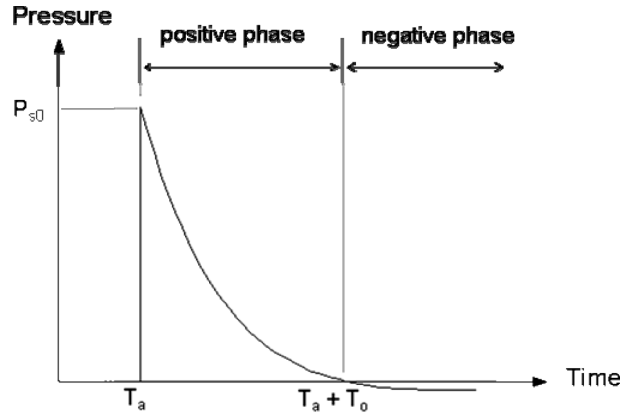
Fig. 1 A typical shape of blast pressure time history

or fluid and contact any structure, causing reflected pressure. The reflected pressure usually varies through the weight and type of explosive, standoff distance (or distance from the detonation), and the incident angle of the wave. The reflected pressure is a blast load on a structure considered in a design and analysis. In addition, the duration and amount of amplification of the reflected pressure can be affected by the shape of target structure or other objects, such as ground, which can produce another reflected blast wave.

FEMA 426 (2003) notes that an explosive event has the following features compared with other hazards such as earthquakes and winds; i) The fact that the intensity of the pressure can be several orders of magnitude greater than other hazards but the explosive pressure decays rapidly with distance from the source results in only a relatively small part of the structure or localized damage; ii) The mass of the structure tends to help mitigating the structural response because the duration of blast wave is very short and the loading is gone by the time the mass of the structure is mobilized. This is the large difference from earthquake loads under which the building mass can cause a resonance and worsen the damage; iii) Because blast loadings are typically over in several miliseconds, higher structural modes which are usually neglected for earthquakes can be excited.

2.2 Simulation of blast load

2.2.1 Direct calculation

The first step in blast related research is to predict blast loads on the structure. For the purpose of blast resistant design, experiment-based direct load-calculating methods have been mostly used to describe the blast pressure on a structure. The variables of a function to represent a blast pressure time history are peak pressure, impulse, arrival time, and the duration of the pressure. These parameters are generally determined by experimental results. Many documents in this field provide graphical form displaying the values of the blast wave parameters as a function of scaled distance after an explosive weight is converted to TNT equivalent weight (TM5-855-1 1990, TM 5-1300 1990).

The shape of blast wave can be represented by linear decay using an approximate triangular equivalents or more realistic exponential decay shown in Fig. 1 based on Friedlander equation which intends to agree with experimental values of blast pressure (Baker 1973). A modified

Friedlander's equation is as follows (Baker 1973)

$$P(t) = P_{s0}\left[1 - \frac{t-T_a}{T_0}\right]\exp^{-A\left(\frac{t-T_0}{T_0}\right)} \tag{1}$$

where $P(t)$ is blast pressure at time t, P_{s0} is peak incident pressure, T_0 is positive phase duration, T_a is arrival time, and A is a decay coefficient.

Peak reflected pressure is given as a function of variables such as peak incident pressure, angle of wave incidence to the surface of an object and shock front velocity etc. Then, reflected impulse proportional to the calibrated peak reflected pressure and the corresponding duration of reflected pressure will be determined (Baker *et al.* 1983, Beshara 1994, Kinney and Graham 1985).

Among the analysis program softwares to predict blast load acting on a structure from a stand-off distance, ConWep program (TM5-855-1 1990) developed by US Army and AtBlast program (ARA, Inc. 2007) funded by US General Services Administration are generally used. These softwares calculate the parameters of blast wave using experimental data and suggested equations based on the data.

2.2.2 CFD simulation

A blast analysis using pressure time history predicted by the ConWep or AtBlast techniques may save computational run time and produces reasonably accurate response. However, it requires the pressure time history calculated at each point of the model segment, which will consume a lot of time and cost; otherwise, the approximate uniform loads on each portion of structure should be provided. However it cannot consider the other complicated effects, such as confinement due to geometry of structure, reflection of multiple blast waves, and shadowing occurring when an object is blocking a surface of structure from direct blast wave (Randers-Pehrson and Banister 1997).

Finite element analysis using computational fluid dynamics (CFD) is recently used for simulating such a complex blast-structure interaction. This numerical method is to transfer blast load to the structure through the coupling between Eulerian or Arbitrary Lagrangian-Eulerian (ALE) model (blast and air) and Lagrangian model (structure) (Souli *et al.* 2000). In Ls-Dyna explicit solver (2005) used in this study, the ALE formulation can solve the largely distorted mesh problems such as the simulation of blast wave propagation through air with the following shcems: a distorted mesh is brought back to the initial mesh in a fixed grid during in Lagrangian step and the materials flow through the intial mesh in Eulerian computations. In the process of the coupling of ALE and Lagrangian elements, contact algorithms decribes the effect of impact of fluid model on structural model with the forumulation for high frequency modes (Zhong 1993). Then, penalty coupling algorithm implemented in the Ls-Dyna program can describe this interaction with the concept shown in Fig. 2. Providing an arbitrary spring between ALE element and Lagrangian element, pressure on a Lagrangian structure and the structure deformation can be calculated using blast
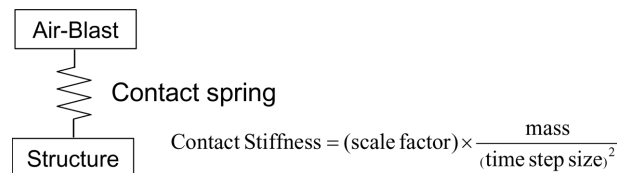

Fig. 2 Penalty coupling concept for blast analysis

pressure transferred through air or fluid and stiffness of the spring. The spring stiffness is determined by mass of Lagrangian model and time step size during analysis. The calculated blast pressure, which is an amplified reflected pressure on a structure, is highly dependent on providing an appropriate penalty factor and coupling points between ALE and structure mesh in the coupling algorithm. It should also be taken into account that the accuracy of numerical results also depends on mesh sizes of both ALE and structure models (Luccioni *et al.* 2006, Mullin and O'Toole 2004).

3. Finite element analysis models

Fig. 3(a) shows a basic finite element model for CFD analysis using the program Ls-Dyna. A detonation cloud was first modelel as a 500kg rectangular TNT charge located at the height of 1.5m above ground. Then, a wide flange steel column with the height of 3.6m, which is assumed to be the column at the first story of steel moment frames, was located 3m away from the TNT in the column weak-axis direction. The ground was assumed rigid. Finally, the air surrounding the TNT,
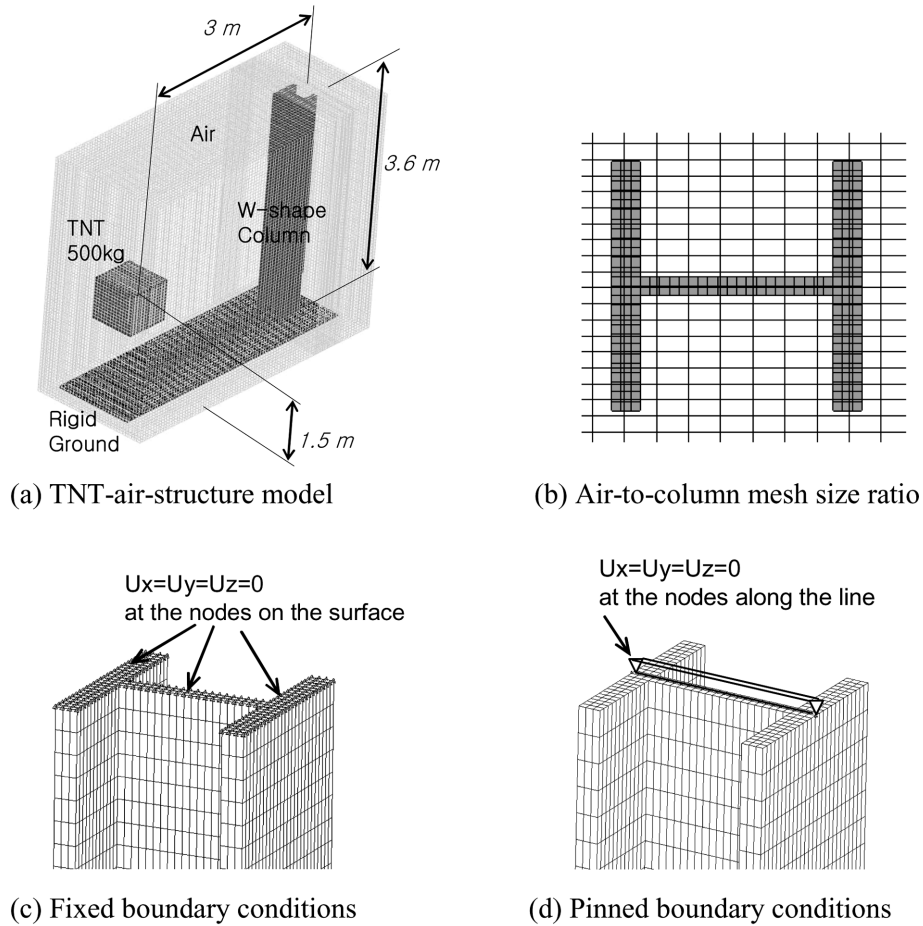

(a) TNT-air-structure model

(b) Air-to-column mesh size ratio

(c) Fixed boundary conditions

(d) Pinned boundary conditions

Fig. 3 Finite element model for parametric study

Table 1 Material properties of TNT, air and steel

TNT		AIR		STEEL	
Density	1630~ 1640 kg/m^3	Initial density (ρ_0)	1.293 kg/m^3	Density	7830 kg/m^3
Detonation velocity	6930 m/s	Initial pressure	1 bar	Static yield stress	345 MPa
Chapman-Jouget pressure	21.0 GPa	Ratio of specific heats (γ)	1.4	Elastic modulus	2.05×10^5 MPa
Internal energy density	7.0 GPa			Hardening modulus	636 MPa

the column, and the ground was modeled. Arbitrary-Lagrangian-Eulerian (ALE) formulation was used for modeling the multi-material fluids of the TNT explosive and the air (fluid part), and Lagrangian formulation was applied for column and ground (structure part). No gravity load on columns was assumed during blast analysis. All meshes were developed using three-dimensional eight-node hexahedron solid elements with one integration point. Undesirable hourglass modes was tried to be prevented by the control option in the Ls-Dyna. For hourglass mode control, the formulation of Flanagan and Belytschko (1981) with the hourglass coefficient of 0.1 was used and the bulk viscosity type was selected to propagate shock waves in solid elements. Penalty coupling algorithm was used to simulate blast load on the structure. The air-to-column mesh size ratio of 3 (see Fig. 3(b)) and two coupling points distributed over each coupled Lagrangian surface segment were provided to achieve a good fluid-structure interaction and an effective computation time as recommended by the Ls-Dyna user's manual (2005).

The TNT detonation product in the fluid part was simulated using an explosive burn material model (*MAT_HIGH_EXPLOSIVE_BURN in Ls-Dyna). The material properties of the TNT explosive to control the release of chemical energy for simulating detonation were taken from Lee *et al.* (1968) as shown in Table 1. Along with the material model, the Johes Wilkins Lee (JWL) equation of state, which is widely used to express pressure-volume-energy response based on experimental data (Lee *et al.* 1973), was adopted to determine the pressure of TNT explosive. The JWL equation of state is as follows

$$p = A\left(1 - \frac{\omega}{R_1 V}\right)e^{-R_1 V} + B\left(1 - \frac{\omega}{R_2 V}\right)e^{-R_2 V} + \frac{\omega E}{V} \tag{2}$$

where p is the pressure, V is the relative volume, E is the internal energy per initial volume, A and B are experimental linear constants, and ω, R_1, R_2 are experimental nonlinear constants (Dobratz and Crawford 1985). The constants of the JWL equation of state for TNT explosive are given in Table 2.

The main fluid material or the air was assumed to be an inviscid ideal gas using *MAT_NULL material with *EOS_LINEAR_POLYNOMIAL equation of state in the Ls-Dyna. These material and equation of state may express a constitutive relation shown in Eq. (3) to be considered without

Table 2 Constants of the JWL equation of state for TNT explosive

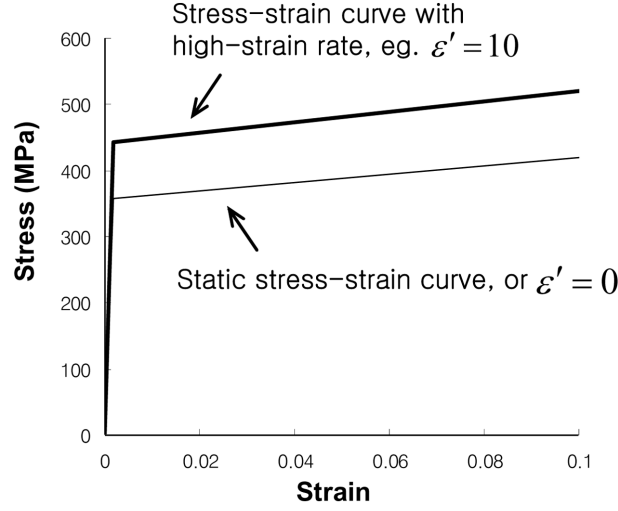|	
A	371.21 GPa
B	3.23 GPa
ω	0.3
R_1	4.15
R_2	0.95

Fig. 4 Stress strain curves with strain rate effect

computing deviatoric stresses under the assumption that the expansion of the blast wave is an adiabatic process.

$$p = (\gamma - 1)\frac{\rho}{\rho_0}E \tag{3}$$

where p is the pressure, ρ is the density, ρ_0 is the initial density, γ is the ratio of specific heats, and E is the internal energy per initial volume. The material properties of air are shown in Table 1 (Ls-Dyna 2005).

The W-section steel columns were modeled considering the dynamic effects resulting from the rapid strain rate due to shock wave of blast explosion. Bilinear stress-strain relationship with kinematic hardening placiticity including strain rate effects was assumed as shown in Fig. 4. The dynamic yield stess (σ'_y) depending on strain rate was calculated using the Cowper-Symonds formulation (1957) as follows

$$\sigma'_y = \left\{1 + \left(\frac{\varepsilon'}{C}\right)^{\frac{1}{q}}\right\}\sigma_y \tag{3}$$

where σ is the static yield stress, ε' is the strain rate and the material constants of $C = 12800$ and $q = 5$ were used based on the least square fit in logarithmic scale of the dynamic yield stress suggested in TM5-1300 (1990). No fracture point of material was assumed to observe the large deformation of the columns. Material properties of steel used in the model are illustrated in Table 1.

In order to determine the column size for parametric analysis, two types of load were imposed on the columns (a point gravity load $P_u = 3{,}202$ kN and a bending moment $M_u = 1{,}561{,}370$ mm-kN). Then, from the LRFD manual (AISC 2001), W14x211 was selected as a typical column in steel moment frames, and W24x162 and W33x152 were selected as alternative deep columns with equivalent strength (see Table 3). The geometric properties of each column were tabulated in Table 4. Their width-to-thickness ratios for both web and flange were intended to meet the seismic compactness limits according to the AISC seismic provisions (2006). Finally, the selected columns were parameterized with the fixed or pinned boundary condtions at both ends of the columns (see

Table 3 Capacities of the selected columns per AISC LRFD

Sections	$Pu/\Phi Pn$	$8/9(M_u/\Phi M_n)$	$(P_u/\Phi P_n)+ 8/9(M_u/\Phi M_n)$
W14×211	0.3	0.7	1.00
W24×162	0.42	0.58	1.00
W33×152	0.49	0.49	0.98

Table 4 Section properties of the selected columns

Sections	h/t_w	$b_f/2t_f$	$Z_x (\times 10^6)$ [mm^3]	$Z_y (\times 10^6)$ [mm^3]
W14×211	11.6	5.06	6.39	3.24
W24×162	30.6	5.31	7.67	1.73
W33×152	47.2	5.48	9.15	1.21

Table 5 Parametric model configuration

Model configuration	Top/bottom boundary conditions
W14×211 ff	fixed
W24×162 ff	fixed
W33×152 ff	fixed
W14×211 ss	pinned
W24×162 ss	pinned
W33×152 ss	pinned

Figs. 3(c), (d) and Table 5). These boundary conditions are expected to represent ideally the rotational capacities of a joint connected to the top of the column and a foundation connected to the bottom of the column.

4. Discussion of numerical studies

4.1 Blast load prediction

Blast wave propagation in the air was simulated using computational fluid dynamics. The blast wave transferred to the structure acted as blast loads on the column through the complex interaction between fluid part (air) and structural part (column). In this section, the feasibility of the calibrated blast loads were evaluated through the comparison with the loads computed using the ConWep and the AtBlast programs. Fig. 5(a) compares the predictions of the reflected pressure time history on the center of the column web at the height of the TNT explosive. It was observed that the peak pressures and the durations of a few thousandths of seconds or milliseconds correspond well with one another. The CFD model has a significant rise time compared to almost negligent ones in the ATBLAST and CONWEP models, and there is a large dip at time 1.5 msec for the CFD model. The discrepancy seems to be somewhat exaggerated due to the small time range (i.e., 0-3 msec) chosen for the figure. In addition, the discrepancy was enlarged by difference in surface rigidities of

(a) Reflected pressure time history
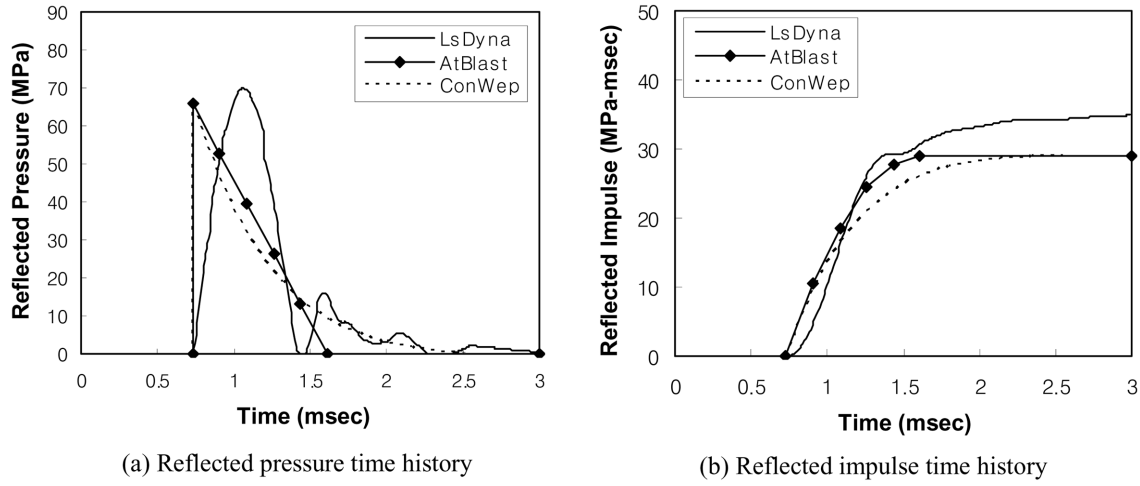
(b) Reflected impulse time history

Fig. 5 Comparison of reflected pressures and impulses at the column web center at the height of TNT
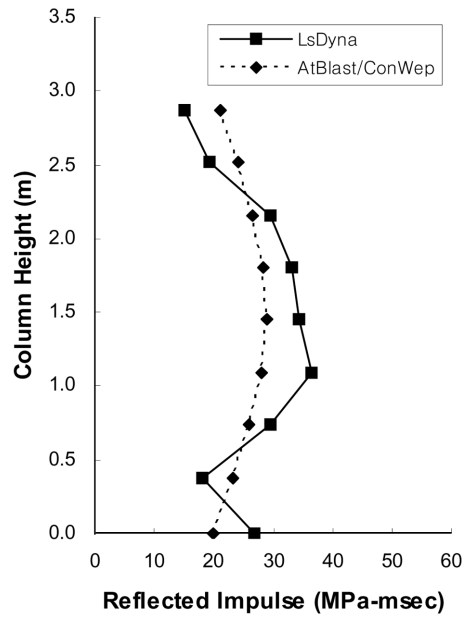

Fig. 6 Comparison of impulse distribution along the column web center line

the two models. For example, web surface of the CFD model is much more flexible than rigid surface assumed by AtBlast or ConWep models. This flexibility may have affected the interaction between column web and blast wave (fluid) and led to the discrepancy in rise and drop. However, as blast load has the shape of a shock wave, its impulse will have a great effect on the response of the structure. In Fig. 5(b) it can be observed that the reflected impulse obtained from the CFD analysis is similar to those obtained from the ConWep and the AtBlast programs up to 1.5 milisecond.

In general, for the blast resistance design of a structural component, the blast pressure or impulse

computed at a point using a well-known equation or program tends to be uniformly distriuted over the component length. However, the nonuniform distribution of the pressure or impulse should be considered in order to achieve the more accurate and reasonable numerial response. Fig. 6 compares the impulse distributions along the column web center line simulated by the AtBlast (or ConWep) and the Ls-Dyna programs. As the impulse profiles of both AtBlast and ConWep model were equal, the results of the AtBlast (or ConWep) and CFD models were compared in the figure. When blast loads on the column were calculated using the AtBlast (or ConWep), the standoff distance and incident angle from the TNT explosive to each point of column were provided accurately. As shown in Fig. 6, both programs predict less impulse at the upper and lower parts of column. The slight difference between the impulse profiles of the AtBlast (or ConWep) and the CFD model may be due to the effects of the rigidity of column web on the blast loading as mentioned above. The smaller impulse at the lower part of the column in the results of the AtBlast (or ConWep) model may be caused by exclusion of the effects of the reflected waves off the ground on the structure.

4.2 Effects of column section size

Shen *et al.* (2002) indicated that the selection of deep columns for steel moment frames in seismic design could help reducing column weight and acheiving the enough column strong-axis moment capacity. In this section, the behavior and damage of the selected W14x211, W24x162, and W33x152 columns subjected to the simulated blast load were observed. The blast load simulated by the ConWep program was applied solely on the surface of the column facing the bomb, while the blast pressure generated by the CFD model was allowed to encompass the perimeter of the column. The column response under the blast loading derived from the AtBlast program was omitted because both impulse distributions from the AtBlast and ConWep program were identical as shown in Fig. 6.

Fig. 7(a) shows that plastic hinges begin to develop at both ends of the column fixed at both ends

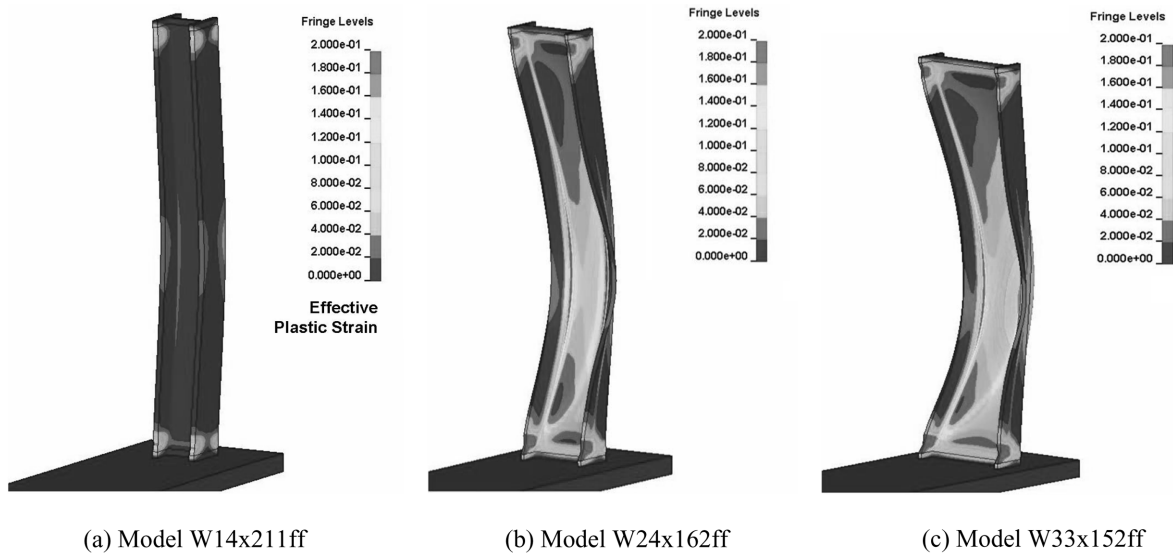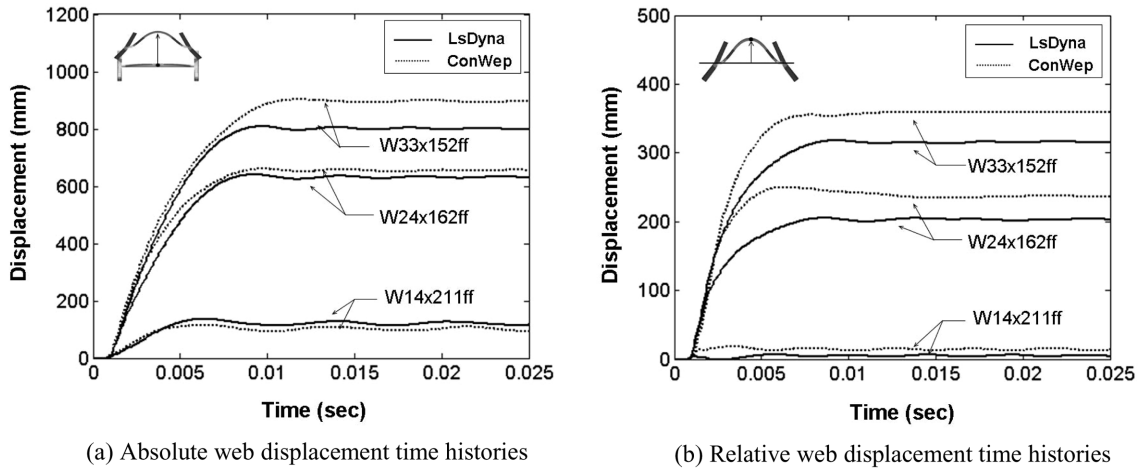(a) Model W14x211ff   (b) Model W24x162ff   (c) Model W33x152ff

Fig. 7 Plastic hinge formation and deformation of columns obtained by CFD analysis model

(a) Absolute web displacement time histories   (b) Relative web displacement time histories

Fig. 8 Comparison of column web displacements obtained by CFD and ConWep programs

(model W14x211ff) due to stress concentration when it is subjected to a blast load simulated by the CFD model. Because the W14x211 column has the larger weak-axis moment capacity than the other deep columns, no plastic hinge at the middle height of the column occurred under the given blast load. Therefore, fracture at the k-line of the column is expected to be prohibited and the entire loss of axial capacity of the column against gravity load is unlikely. However, Figs. 7(b) and (c) show that the alternative deep columns (models W24x162ff and W33x152ff) would develop plastic hinge at the middle height of the columns due to their smaller weak-axis moment capacities. The stress redistribution and large deformation resulted in the damage on flange at both ends of the column W33x152 which has the largest web width-to-thickness ratio and the smallest Z_y. Fracture at the k-line of the deep columns following the large deformation is also expected.

The blast responses of columns resulting from both methods were compared in Figs. 8 and 9. Fig. 8(a) shows the absolute displacement time histories of the web center at the middle height of the columns. As expected, the deepest column W33x152ff had the largest displacement due to blast load on the largest web area. It can be observed in the figures that both models provided the similar responses of the column W14x211ff, but resulted in different responses in the deep columns W24x162ff and W33x152ff. As the deeper columns have the larger surface facing the bomb, more differences were observed in the results of the ConWep model (where the blast load was loaded solely on the surface) and the results of the CFD model (representing the complex interaction of blast pressure emcompassing the perimeter of the column). Furthermore, as shown in Fig. 8(a), the absolute displacement of the deepest column W33x152 obtained by both models have exceeded the global ductility limit (800 mm). Fig. 8(b) shows the relative web displacement time histories with respect to the flange displacement (or web displacement excluding column rigid body motion), where little relative displacement occurred in the W14x211ff and the largest relative displacement was observed in the column W33x152ff. The main reason for the difference can be explained by the different web width-to-thickness ratios summarized in Table 4. However, there was no big difference in effective plastic strains at the k-lines of the W24x162ff and the W33x152ff as shown in Fig. 9. It can be observed in Fig. 9 that the plstic strains at the k-lines obtained from both models are similar to each other; as time goes by the results from ConWep become slightly larger than those obtained by CFD model. Therefore it is not always expected that the magnitude of absolute or
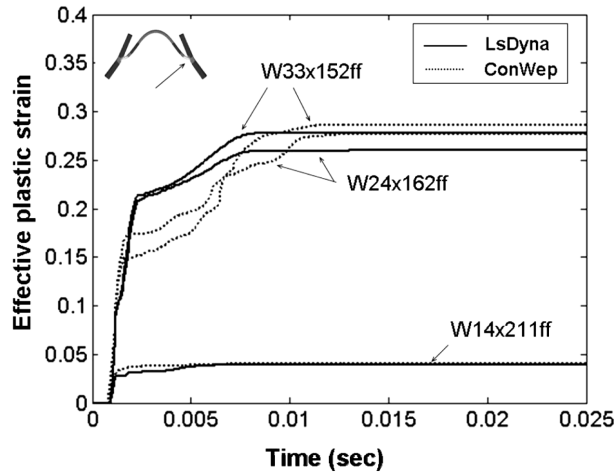
Fig. 9 Comparison of effective plastic strains at k-line obtained by CFD and ConWep programs

relative web displacement under a blast load is proportional to the magnitude of strain concentration and the possibility of fracture at the k-line.

4.3 Effects of boundary conditions

The effects of boundary condtion on the deformation and damage of the columns under the simulated blast load were illustrated in Fig. 10. The relative web displacements of the columns pinned at both ends were a little bit smaller than but not quite different from those of the columns fixed at both ends as shown in Fig. 10(a). However, Fig. 10(b) shows that the maximum values of effective plastic strain at the k-line of the pinned columns are much larger than those of the fixed columns. If the steel material is assumed to be failed at the effective plastic strain of 0.4, the pinned deep columns (models W24x162ss and W33x152ss) would experience fracture at the k-line. The

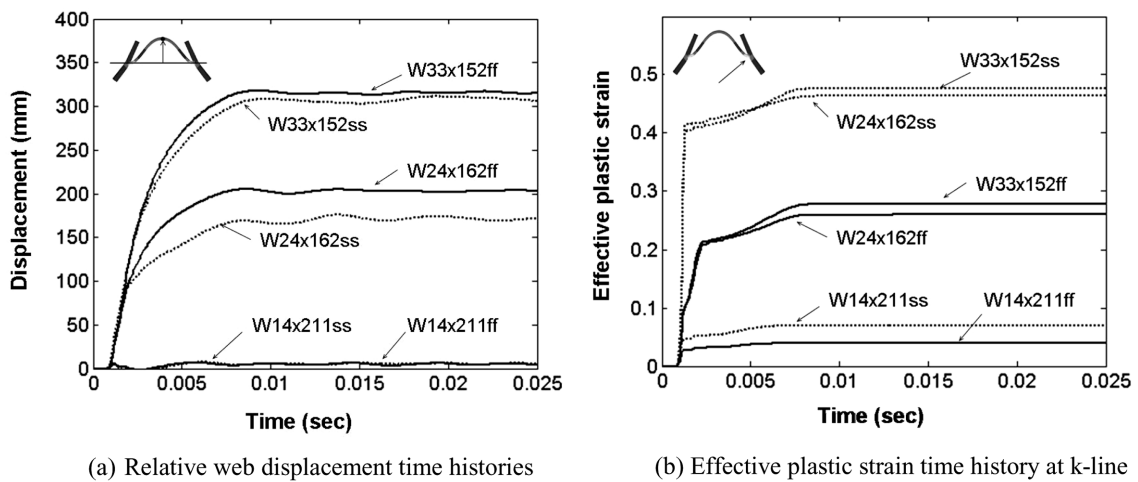(a) Relative web displacement time histories   (b) Effective plastic strain time history at k-line

Fig. 10 The effects of boundary conditions on displacement and strain of columns

plastic deformation of the columns pinned at both ends was concentrated at the middle, but the plastic deformation of the columns fixed at both ends spreads out to both ends. This resulted in the decrease in strain concentration at the k-line of columns. It is again noted that the column deformation is not directly related to the fracture due to strain concentration at the k-line.

5. Conclusions

In this study blast loads were simulated by high-fidelity finite element analysis using computational fluid dynamics (CFD) and the behavior of wide flange steel columns subjected to the blast loads was observed. The results of this study are summarized as follows:

1) The blast loads (pressure and impulse) simulated through fluid structure interaction in CFD analysis were compared with the loads calculated through experiment-based direct method using the program code AtBlast or ConWep. The validity of the predicted blast load and the advantage of CFD analysis method were evaluated.

2) In order to estimate the blast resistance of the wide flange section columns, parametric numerical analysis was conducted with a W14x section as a typical column and W24x and W33x sections as alternative deep columns. It was observed that the deep columns selected based on seismic resitance can be highly vulnerable to blast load in the column weak-axis direction. It was also observed that the web width-to-depth ratio was closely related to the deformation and failure at the k-line of columns under blast load.

3) The effect of boundary condition of column ends on behavior and failure of columns was also observed; the plastic deformation of the columns pinned at both ends was concentrated at the middle and resulted in larger strain concentration at the column k-line. It was also indicated that the magnitude of the column web displacement was not directly related to the magnitude of strain concentration (or the possibility of fracture) at the k-line.

This study showed that the analytical approach using CFD modeling is reasonable and effective to understand the nature of blast wave and complex interaction between blast load and behaviour of a steel column.

Acknowledgements

References

AISC (2001), *Manual of Steel Construction: Load and Resistance Factor Design*, 3rd edtition, American Institute of Steel Construction, Chicago, IL.
AISC. (2006), *Seismic Provisions for Structural Steel Buildings*, American Institute of Steel Construction, ANSI/ AISC 341-05, Chicago, IL.
Applied Research Associates (ARA), Inc. (2007). *AtBlast program*, Protective Glazing Council, <http:// www.protectiveglazing.org>
Baker, W.E. (1973), *Explosions in Air*, University of Texas Press. Austin, TX.

Baker, W.E., Cox, P.A., Westine, P.S., Kulesz, J.J. and Strehlow, R.A. (1983), *Explosion Hazards and Evaluation*, Elsevier.

Beshara, F.B.A. (1994), "Modelling of blast loading on aboveground structures - I. General phenomenology and external blast", *Comput. Struct.*, **51**(5), 585-596.

Cowper, G.R. and Symonds, P.S. (1957), *Strain Hardening and Strain Rate effect in the Impact Loading of Cantilever Beams*, Brown University, Division of Applied Mathematics Report No. 28.

Dobratz, B.M. and Crawford, P.C. (1985), *LLNL Handbook of Explosives*, Lawrence Livermore National Laboratory, Livermore, CA.

FEMA-426. (2003), *Reference Manual to Mitigate Potential Terrorist Attacks Against Buildings*, Federal Emergency Management Agency, Report No. 426, Washington D.C.

Flanagan, D.P. and Belytschko, T. (1981), "A uniform strain hexahedron and quadrilateral and orthogonal hourglass control", *Int. J. Numer. Meth. Eng.*, **17**, 679-706.

Hamburger, R.O. and Whittaker, A.S. (2003), "Design of steel structures for blast-related progressive collapse resistance", American Society of Civil Engineers, <http://www.aisc.org> (Nov. 15, 2005).

Kang, K.W. and Liew, J.Y.R. (2006), "Blast response of steel-concrete composite structures, international colloquium on stability and ductility of steel structures", *SDSS2006*, Lisbon, Portugal, 861-868.

Kinney, G.F. and Graham, K.J. (1985), *Explosive Shocks in Air*, 2nd edition, Berline: Springer Verlag.

Ls-Dyna (1998), *LS-DYNA Theoretical Manual*, Livermore Software Technology Corporation, Livermore, CA.

Ls-Dyna (2005), *LS-DYNA Keyword User's Manual*, version 970, Livermore Software Technology Corporation, Livermore, CA.

Lee, E.L., Hornig, H.C. and Kury, J.W. (1968), *Adiabatic Expansion of High Explosive Detonation Products*, UCRL-50422, University of California, Lawrence Livermore National Laboratory, Livermore, CA.

Lee, E., Finger, M. and Collins, W. (1973), *JWL Equation of State Coefficients for High Explosives*, UCID-16189, University of California, Lawrence Livermore National Laboratory, Livermore, CA.

Luccioni, B., Ambrosini, D. and Danesi, R. (2006), "Blast load assessment using hydrocodes", *Eng. Struct.*, **28**, 1736-1744.

Marchand, K.A. and Alfawakhiri, F. (2005), *Facts for Steel Buildings: Blast and Progressive Collapse*, American Institute of Steel Construction (AISC), Chicago, IL.

Mullin, M.J. and O'Toole, B.J. (2004), "Simulation of energy absorbing meterials in blast loaded structures", *8th International LS-DYNA Users Conference*, Penetration/Explosive, Dearborn, MI, May 2-4.

Randers-Pehrson, G. and Banister, K.A. (1997), *Airblast Loading Model for DYNA2D and DYNA3D*, ARL-TR-1310.

Shen, J.H.J., Astaneh-Asl, A. and McCallen, D.B. (2002), *Steel Tips: Use of Deep Columns in Special Steel Moment Frames*, American Institute of Steel Construction.

Souli, M., Ouahsine, A. and Lewin, L. (2000), "ALE formulation for fluid-structure interaction problems", *Comput. Meth. Appl. Mech. Eng.*, **190**(5-7), 659-675.

TM 5-855-1. (1990), *Fundamentals of Protective Design for Conventional Weapons*. U.S. Department of the Army, Washington D.C.

TM 5-1300. (1990), *Structures to Resist the Effects of Accidental Explosions*, Joint Departments of the Army, Air Force and Navy, Washington D.C.

Zhong, Z.H. (1993), *Finite Element Procedures for Contact-impact Problems*, Oxford University Press, Oxford.